Research Square

Preprints are preliminary reports that have not undergone peer review.
They should not be considered conclusive, used to inform clinical practice,
or referenced by the media as validated information.

Thermo-hydraulic and thermal stress performance of a shell-and-tube heat exchanger under varying tube-wall thickness: Coupled CFD–FEA investigation

Oku Nyong

nyong.oku@gmail.com

University of Cross River State

Victor Udeme

Joseph Sarwuan Tarka University

Raymond Ana

University of Calabar

Gideon Ogban-Ekpe

University of Calabar

Ukpabio Eyo

University of Cross River State

Eward Obi

University of Calabar

Research Article

Keywords: HTC, computational fluid dynamics, tube thickness, pressure drop, thermal stress, solidworks flow simulation

Posted Date: November 9th, 2026

DOI: https://doi.org/10.21203/rs.3.rs-11107477/v1

License: This work is licensed under a Creative Commons Attribution 4.0 International License.
Read Full License

Additional Declarations: No competing interests reported.

Thermo-hydraulic and thermal stress performance of a shell-and-tube heat exchanger under varying tube-wall thickness: Coupled CFD–FEA investigation.

Nyong, Oku Ekpenyong[1], Udeme, Victor Akpan [3], Ana, Raymond[2], Ogban-Ekpe, Gideon Adonokpem[2], Eyo, Ukpabio Ekpenyong[1] ,and Obi, Edward Asu[2].

[1]Thermofluid, Combustion, and Renewable Energy System Research Group, Department of Mechanical Engineering, University of Cross River State, P.M.B. 1123, Calabar, Nigeria.

[2]Department of Mechanical Engineering, University of Calabar, P.M.B 1115, Calabar, Nigeria.

[3]Department of Mechanical Engineering, Joseph Sarwuan Tarka University, Benue State, Nigeria.

Corresponding author: nyong.oku@gmail.com

Abstract

Shell-and-tube heat exchangers (STHE) are widely used in industries because of their efficiency, simplicity, and high-pressure drop capability. However, their tubes are prone to failure modes such as erosion, thermal fatigue, vibration, pressure impact, and fouling, which over time affect their operational performance and increase the cost of maintenance, repair, or replacement. The tube wall thickness is a critical design parameter in shell-and-tube heat exchangers, influencing the thermal performance, hydraulic behaviour, and structural integrity. This study investigates the coupled effects of tube thickness on the overall heat transfer coefficient (HTC), tube-side pressure drop, and thermal stress using SOLIDWORKS Flow Simulation and structural analysis tools (ver. 2025). The geometry was modeled in a three-dimensional (3D) model with two passes and water as the working fluid. The SOLIDWORKS Flow Simulation tool (ver. 2025) was used to perform the computational fluid dynamics (CFD) simulation on the model domains, adopting the k-ε turbulence model and structural analysis tools. A parametric analysis was conducted by varying the tube thickness while maintaining constant operating conditions. In the simulation, the tube thickness was increased from 0.5 to 2.0 mm. The results showed that at a higher tube thickness, there was a reduction in the overall heat transfer coefficient and thermal stress, whereas a substantial increase in the pressure drop at the tube side of the shell-and-tube heat exchanger was observed. When the tube thickness increased from 0.5 to 2.0 mm, the HTC from 839 to 682.9 W/m^{2,} amounting to an 18.6% in HTC, whereas the maximum von Mises stress decreased by approximately 14.9% when the tube-wall thickness increases from 0.5 mm to 2.0 mm. Consequently, increasing the tube wall thickness from 0.5 to 2.0 mm resulted in a substantial increase in pressure drop from 65.3 to 3352 Pa, corresponding to an increase of approximately 50.33% (51.3-fold), and the maximum von Mises stress decreased from approximately 1.575×10^8 Pa at 0.5 mm wall thickness to 1.34×10^8 Pa at 2.0 mm, representing an overall reduction of approximately 14.9%. This indicates that the pressure drop is considerably more sensitive to the tube wall thickness than the thermal performance parameters. This finding helps in adopting the appropriate tube thickness in the design of shell-and-tube heat exchangers.

Keywords: HTC, computational fluid dynamics, tube thickness, pressure drop, thermal stress, solidworks flow simulation.

Nomenclature

Symbols	**Notations**
Q	heat duty (W)
d	diameter (m)

$\dot{m}$	Mass flow rate (kg/s)
T	Temperature (^oC)
C_L	Shell side clearance (m)
L_{pt}	Tube pitch
D_b	Bundle diameter (m)
D_s	Shell diameter (m)
D_e	Shell hydraulic diameter (m)
C_p	Heat capacity (J/kg. ^oC)
Re	Reynold number
U	Overall heat transfer coefficient, (W/m^2. ^oC)
N_t	Number of tubes
K_1, n_1	Coefficient
P_t	Tube pitch
ΔT_{lm}	logarithmic mean temperature difference
P,R	Constant associated with correction factor chart
h	Heat transfer coefficient
R_f	fouling resistance
F	Correction factor (m^2.K/W)
L	Length of tube (m)

K	Thermal conductivity (W/m^{2}K)
A	Area (m^2)
Pr	Prandtl number
V	Flow velocity
S_A	heat transfer surface area (m^2)
N_{passes}	Number of passes
E	Young modulus
B	Baffle spacing
ΔP	Pressure drop (Pa)
f	Friction factor
P_B	buoyancy force
Q_H	specific heat release (or absorption) per unit volume
q_i	diffusive heat flux
h	thermal enthalpy
k	Karman constant
A_v	Van Driest coefficient
y^+	dimensionless wall distance
u^+	dimensionless velocity
Creek letters	

$\boldsymbol{\rho}$	Density
η	Pump efficiency
$\boldsymbol{\mu}$	Fluid dynamics viscosity
$\boldsymbol{\varepsilon}$	turbulence dissipation rate
$\boldsymbol{k}$	turbulent kinetic energy
λ_i	eigenvalue of the thermal conductivity tensor
τ^R	Reynolds-stress tensor
δ	Kronecker delta function
υ	Poisson's ratio
α	Coefficient of thermal expansion
Subscript	
s,i	Shell inlet
s,o	Shell outlet
t,i	Tube inlet
t,o	Tube outlet
w	Wall
Acronyms	
CFD	Computational fluid dynamics
LMTD	logarithmic mean temperature difference
BDC	Bundle diameter clearance
LSSTHE	laboratory-scale shell-and-tube heat exchanger
ASTM	American society for Testing and materials
QUICK	Quadratic Upstream Interpolation for Convective Kinematics
FVM	finite volume method
HTC	Heat transfer coefficient
STHE	Shell and tube heat exchanger

1.0 Introduction

Shell-and-tube heat exchangers (STHEs) remain the predominant technology for thermal energy exchange across a vast spectrum of industrial sectors, including petrochemical processing, power generation, heating, ventilation, and air conditioning (HVAC) systems, food processing, and other energy-intensive applications. [1]. Their importance has increased with the growing emphasis on energy efficiency and process intensification, since the performance of a heat exchanger directly affects the energy consumption, operating cost, and overall efficiency of the system in which it is installed. STHE has remained an active research area because of the continuing need to improve heat-transfer performance while limiting pressure losses and maintaining mechanical reliability. Recent literature has increasingly emphasized the concept of thermo-hydraulic performance, in which heat-transfer enhancement is evaluated together with the corresponding hydraulic penalty. Recent reviews have consequently identified heat-transfer enhancement, pressure-drop reduction, and overall thermo-hydraulic performance as continuing priorities in shell-and-tube heat-exchanger research [2]. Their widespread adoption is attributed to their robust mechanical design, high-pressure tolerance, and versatility in handling diverse fluid pairs. A comprehensive review by Marzouk et al. [2] showed that a substantial proportion of recent STHE research has concentrated on heat-transfer enhancement, while pressure drop, overall heat-transfer coefficient, and thermo-hydraulic performance remain important evaluation criteria [2]. Despite their mature engineering status, the continuous demand for enhanced energy efficiency and operational reliability necessitates rigorous optimization of their geometric parameters. Among these parameters, tube wall thickness emerges as a critical variable that fundamentally governs the coupled phenomena of conjugate heat transfer and structural mechanics. Tube-wall thickness has received comparatively less systematic attention despite its simultaneous influence on thermal, hydraulic, and structural behavior. The optimization of tube wall thickness is not merely a geometric adjustment but a complex multidisciplinary challenge that requires balancing minimal thermal resistance against sufficient mechanical integrity under severe operating conditions [3]. The significance of tube wall thickness in STHE performance is multifaceted, influencing both thermohydraulic efficiency and structural reliability. From a thermohydraulic perspective, the tube wall acts as a conductive barrier between the shell-side and tube-side fluids. Variations in wall thickness directly alter the overall thermal resistance network, thereby impacting the global HTC and the local temperature gradients that drive heat flux [3]. While thinner walls reduce conductive resistance and potentially enhance heat transfer rates, they may compromise the structural stability of the tube, increasing susceptibility to vibration, buckling, and mechanical failure under pressure loads [1]. Conversely, thicker walls provide greater mechanical strength and resistance to corrosion and erosion but introduce additional thermal resistance, which can diminish the overall thermal performance of the exchanger [4]. This trade-off is further complicated by the presence of complex flow patterns, turbulence, and potential fouling, which interact with the geometric constraints imposed by the tube dimensions [5].

In addition to thermohydraulic considerations, tube wall thickness plays a pivotal role in determining the thermal stress distribution and fatigue life of the heat exchanger components. During operation, STHEs are subjected to significant thermal gradients and pressure differentials, leading to the development of von Mises stresses and thermal deformations within the tube bundle [6]. These stresses are particularly pronounced in applications involving high-temperature fluids, such as molten salt solar collectors or coal-water slurry preheaters, where uneven temperature distributions can induce severe thermal fatigue [7]. The structural implications of tube-wall thickness are equally important. During heat-exchanger operation, the tubes are exposed to temperature differences and pressure loading. The resulting thermal expansion and mechanical loading can generate stresses and deformation within the tube wall. Consequently, structural assessment should consider not only the magnitude of temperature but also the resulting thermal gradients and constraints. Increasing wall thickness can alter the stiffness and load-bearing capacity of the tube, while changes in the temperature field can modify the magnitude and distribution of thermally induced stresses. Recent thermo-mechanical investigations have demonstrated that temperature and operating pressure can substantially influence the structural response of shell-and-tube heat exchangers. Delibaş and Yılmaz [8] demonstrated the importance of considering thermo-mechanical behavior in assessing the performance and service life of shell-and-tube heat exchanger components [8]. Likewise, Serttikul et al. recently used finite-element analysis to investigate conjugate heat transfer and structural behavior in a shell-and-tube heat exchanger and demonstrated the influence of operating temperature on stress distribution and thermal expansion. These studies suggest that thermal performance alone cannot provide sufficient information for determining the suitability of a tube-wall configuration. A wall thickness that provides favorable heat-transfer characteristics may not necessarily provide the most favorable structural response.

Numerical studies utilizing fluid-structure interaction (FSI) models have demonstrated that the mechanical performance of heat exchangers is highly sensitive to wall thickness, with thinner tubes exhibiting higher deformation and stress concentrations under identical thermal loads [6]. Furthermore, the cyclic nature of many industrial processes

exacerbates these effects, making the prediction of remaining useful life and the establishment of plugging criteria based on wall thickness reduction essential for maintaining operational safety [4]. Numerical simulations using FSI models reveal that thinner tubes are more susceptible to deformation and higher von Mises stresses under identical thermal loads, potentially leading to buckling or fatigue failure [6]. Conjugate heat transfer models are essential for capturing the continuous temperature field across the fluid-solid interface, providing a more realistic representation of thermal performance than traditional segregated approaches [9]. The complexity of these coupled phenomena renders traditional empirical correlations insufficient for accurate performance prediction, necessitating the use of advanced numerical approaches. CFD coupled with Finite Element Analysis (FEA) has become the standard for investigating the multifaceted effects of tube wall thickness [5]. CFD simulations enable the detailed resolution of flow fields, temperature distributions, and pressure drops, capturing intricate phenomena such as boundary layer separation and recirculation zones [10-12]. When integrated with FEA, these thermal fields can be mapped onto structural models to compute stress and deformation, allowing for a comprehensive assessment of mechanical integrity [6]. Recent advancements include the use of porous media approaches to optimize shell-side flow and conjugate heat transfer models to accurately resolve fluid-solid interfaces [6, 9]. These numerical methods offer significant advantages over experimental trials by enabling systematic parametric studies at a fraction of the cost and time [13, 14].

Conversely, excessively thick tubes may induce higher residual stresses during manufacturing and increase the overall weight and cost of the exchanger without proportional gains in safety [7]. The analysis of thermal stress is further complicated by transient operating conditions, such as startup and shutdown cycles, which introduce thermomechanical fatigue. Studies on high-temperature applications demonstrate that wall thickness significantly influences the fatigue life of components, with thicker walls often exhibiting better resistance to thermal shock but potentially higher peak stresses due to constrained expansion [15]. In marine and offshore applications, where STHEs are subjected to dynamic loads and varying ambient conditions, the structural response to wall thickness variations is critical for ensuring long-term reliability [13]. Numerical approaches that couple thermal field simulations with structural mechanics allow for the prediction of stress concentration zones, enabling designers to optimize wall thickness to minimize peak stresses while maintaining adequate heat transfer performance [6]. Additionally, FSI models have been utilized to investigate the mechanical performance of heat exchangers under different loads, providing insights into stress distribution mechanisms and failure modes [6]. The integration of these numerical tools allows for a holistic evaluation of STHE performance, bridging the gap between theoretical design and practical application [16].

The accurate assessment of tube wall thickness effects relies on advanced numerical methodologies that integrate CFD for fluid dynamics and heat transfer with finite element analysis (FEA) for structural analysis. CFD provides an effective means of investigating this problem because it permits the detailed prediction of velocity, pressure, and temperature distributions within complex heat-exchanger geometries. The importance of simultaneously considering heat transfer and pressure loss has also been demonstrated through CFD studies. Recent research has demonstrated the increasing application of three-dimensional CFD to shell-and-tube heat exchangers. Bahiraei et al. [17] investigated a shell-and-tube exchanger equipped with modified helical baffles and found that increasing Reynolds number enhanced heat-transfer characteristics but also increased pressure loss [17]. Biçer et al. [18] used CFD together with Taguchi methodology to investigate baffle configuration and demonstrated that appropriate geometric modification could improve heat transfer while reducing pressure loss [18].These studies establish that exchanger performance is governed by competing thermal and hydraulic mechanisms. Abeykoon [19] demonstrated the computational burden associated with full-scale CFD simulations of shell-and-tube heat exchangers and proposed a semi-full-scale modeling approach based on the repeated geometry of exchanger tube bundles. The study emphasized that the large number of tubes and baffles can make full-scale simulations computationally demanding [19]. Wang et al. [11] developed three-dimensional CFD coupling approaches for shell-and-tube heat exchangers and highlighted the importance of accurately resolving the coupled flow and heat-transfer processes on the shell and tube sides [20]. More recent CFD studies have continued to investigate the influence of Reynolds number, fluid properties, flow arrangement, and exchanger geometry on heat-transfer and hydraulic characteristics [21]. Despite these advances, the majority of recent numerical investigations have focused on variables such as baffle configuration, tube arrangement, working-fluid modification, flow enhancement, and operating conditions. These studies establish CFD as a suitable approach for the present investigation. Nevertheless, CFD results are sensitive to mesh resolution, turbulence modeling, boundary conditions, and convergence criteria. Consequently, a reliable CFD investigation of tube-wall thickness must incorporate an appropriate mesh-independence study and numerical verification before physical trends can be interpreted. Grid independence studies are crucial in these simulations to ensure that the resolution of the boundary layers and the solid domain is sufficient to capture steep thermal and velocity gradients near the tube walls [12, 22]. Furthermore, the choice of turbulence model and boundary conditions significantly impacts the accuracy of thermohydraulic predictions [12]. Comparative studies of turbulence models, such as k-epsilon and k-omega, indicate

that certain models offer superior convergence and accuracy for complex flow fields within STHEs, particularly when evaluating the impact of geometric modifications like wall thickness [23]. Recent advancements in numerical modeling have facilitated the use of porous media approaches and conjugate heat transfer models to optimize STHE designs with greater precision [10]. These methods enable researchers to perform parametric studies, systematically varying tube wall thickness and other geometric parameters to identify optimal configurations [24]. For example, numerical studies have employed various turbulence models to evaluate the impact of geometric modifications on heat transfer rates and pressure drops, highlighting the importance of model selection in achieving accurate results [23]. The review also identified the need for further numerical investigation and improved theoretical treatment of heat-transfer enhancement approaches [2]. A particularly relevant study was reported by Krisdiyanto et al.[25] who investigated the effect of tube thickness on a shell-and-tube heat exchanger. Their study considered heat transfer, pressure drop, and stress analysis and demonstrated that tube thickness can simultaneously influence the thermal, hydraulic, and structural characteristics of the exchanger [25]. Although considerable research has been devoted to improving the thermal and hydraulic performance of shell-and-tube heat exchangers through modifications of operating conditions, tube geometry, tube length, shell diameter, baffle configuration and flow arrangement, comparatively limited attention has been given to the systematic influence of tube wall thickness on the coupled thermo-hydraulic and thermo-mechanical behaviour of the exchanger. In conventional heat exchanger design, tube wall thickness is generally selected primarily from mechanical requirements such as pressure containment, allowable stress, corrosion allowance and fabrication considerations. Consequently, its simultaneous influence on heat transfer, fluid-flow resistance, temperature distribution and thermally induced stress has not been sufficiently integrated into the design assessment of STHEs.

A further gap exists in understanding the coupled consequences of increasing tube wall thickness while maintaining a constant tube outside diameter. Under this condition, increasing wall thickness necessarily reduces the tube internal diameter, thereby altering the available flow area, fluid velocity, Reynolds number, frictional losses and tube-side pressure drop. At the same time, the increase in wall thickness introduces additional conductive thermal resistance, which can modify the temperature difference across the tube wall and consequently affect the overall heat transfer coefficient. These competing thermal and hydraulic effects mean that tube thickness cannot be considered solely as a structural design parameter. A thickness that improves structural rigidity may simultaneously increase flow resistance and thermal resistance, potentially producing a trade-off between heat-transfer performance, pumping requirement and structural response. Moreover, previous investigations have generally treated thermo-hydraulic performance and structural/thermal-stress behaviour as separate design problems. There is comparatively limited work that systematically establishes the relationship between tube wall thickness, heat transfer coefficient, temperature distribution, pressure drop and Von Mises stress within a common three-dimensional numerical framework. In particular, the manner in which changes in tube wall thickness modify the thermal field and, subsequently, the thermally induced stress distribution within the tube and critical regions of the heat exchanger remains insufficiently quantified [5, 26]. This represents an important knowledge gap because the thermal performance of an exchanger cannot be considered independently of its structural reliability when subjected to simultaneous temperature and pressure loading.

The present study addresses this gap by developing a three-dimensional conjugate heat-transfer and thermo-mechanical numerical framework to systematically investigate the effect of tube wall thickness on the performance of a shell-and-tube heat exchanger. Unlike studies that evaluate thickness principally from a mechanical-design perspective, the present investigation considers tube wall thickness as a coupled thermal, hydraulic and structural design variable. Tube thickness is varied systematically while maintaining the tube outside diameter, allowing the effects of the resulting change in internal diameter to be directly evaluated.

The novelty of the study therefore lies in the integrated quantification of the competing effects of tube wall thickness on heat transfer, pressure drop, temperature distribution and thermally induced Von Mises stress within the same STHE configuration. The study establishes the physical links between wall thickness and internal flow diameter, between internal diameter and hydraulic resistance, between wall thickness and thermal resistance, and between the resulting temperature field and thermo-mechanical stress response. This provides a more comprehensive understanding of how tube thickness influences overall exchanger behaviour than an assessment based on thermal or structural performance alone. A further contribution is the identification of the trade-off between thermal performance, hydraulic penalty and structural response associated with different tube wall thicknesses. Rather than assuming that either a thinner or thicker tube is inherently preferable, the study provides a quantitative basis for identifying a suitable thickness range according to the combined performance requirements of the exchanger. The resulting framework can therefore support tube-thickness selection based not only on mechanical integrity but also on heat-transfer effectiveness and hydraulic performance. Accordingly, the principal contribution of this work is the development of a coupled thermo-hydraulic–thermo-mechanical assessment methodology for tube wall thickness selection in shell-

and-tube heat exchangers, providing quantitative relationships between tube thickness, internal flow area, heat-transfer characteristics, pressure loss, temperature distribution and Von Mises stress. The findings are intended to provide a more comprehensive design basis for selecting tube wall thickness in STHEs where thermal performance, hydraulic efficiency and structural integrity must be considered simultaneously.

2.0 Numerical Modeling

2.1 Geometrical domain and geometry

Three-dimensional numerical models of the two-pass STHE was developed in SOLIDWORKS 2025. The exchanger consisted of a 127 mm internal-diameter shell containing 30 copper tubes arranged in a square pattern. The shell and tubes had an effective length of 800 mm. Twelve baffles with a diameter of 123 mm and thickness of 4 mm were distributed at 61.5-mm intervals. Water was used as the working fluid on both the shell and tube sides. The tube external diameter was maintained at 9.5 mm, while the tube-wall thickness was parametrically varied between 0.50 and 2.00 mm. Fig. 1. Shows the side view of the heat exchanger.

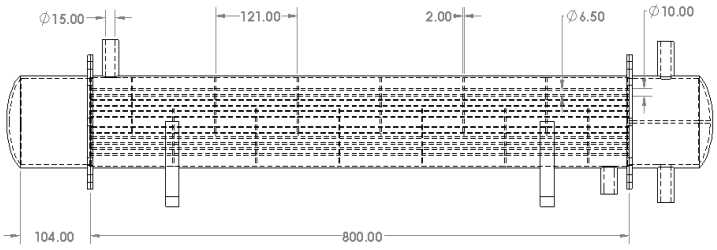


Fig. 1: side view of the STHE

Fig. 2 presents the different tube wall thicknesses considered in this study. The outer diameter is fixed at 9.5 mm, while the internal diameter is varied according to the equation 1.

$$D_i = D_o - 2t \tag{1}$$

Where the D_i and D_o are the internal and outer tube diameters, while t is the tube thickness. Table 1 shows the variations in the internal diameter of the tubes.

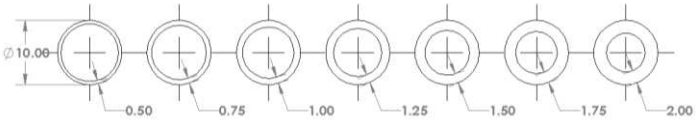


Fig. 2: The dimension of the tube thickness ranges from 0.5 mm to 2.0 mm.

Table 1. Variations in internal diameter of tube wall.

Wall thickness	Internal diameter
0.50 mm	8.50 mm
0.75 mm	8.00 mm
1.00 mm	7.50 mm

1.25 mm	7.0 mm
1.50 mm	6.50 mm
1.75 mm	6.00 mm
2.00 mm	5.50 mm

The detailed geometrical parameters and design conditions of STHE are displayed in Table 2.

Table 2.0: Computational domain and geometry.

Parameter	**Description**
Shell diameter. D_S	127 mm
Tube Outer diameter, d_o	9.5 mm
Number of tubes, N_t	30
Length of Tube, L_t	800 mm
Length of Shell, L_S	800 mm
Diameter of Baffles, B_{dia}	123 mm
Baffle cuts, B_C	25%
Number of baffles, N_B	12
Sheet thickness, S_x	4 mm
Baffle spacing, B_s	61.5 mm
Tube bundle arrangement	Square

2.2 Computational Mesh independence and Grid convergence study

The 3D geometry of the STHE was prepared and meshed using the SolidWorks Flow Simulation Meshing tool (ver. 2025) starting with the global mesh settings, and then gradually using the local mesh setting to refine the region of interest. A mesh independence study was conducted to determine an appropriate computational mesh density for the shell-and-tube heat exchanger simulations. Four progressively meshes from coarse to fine meshes comprising 123,964, 331,896, 828,006 and 1,698,019 computational cells were generated while maintaining identical geometry, thermophysical properties, boundary conditions, turbulence model and numerical convergence criteria. The shell-side outlet temperature T_{co} and LMTD were selected as the monitoring parameters because of their direct relevance to the thermal performance of the heat exchanger. As the mesh density increased, both monitored parameters exhibited progressively smaller changes. The changes in T_{co} between successive meshes were 4.17%, 2.82% and 0.73%, respectively, whereas the corresponding changes in LMTD were 11.49%, 6.43% and 1.92%. The relatively large variations observed between the coarser meshes demonstrate the sensitivity of the thermal solution to spatial discretization. However, refinement from 828,006 to 1,698,019 cells resulted in only a 0.73% change in T_{co} and a 1.92% change in LMTD, indicating that the solution was approaching mesh-independent behaviour. To further quantify the effect of spatial discretization, a Grid Convergence Index (GCI) analysis was performed using the three finest meshes. The characteristic mesh size was determined from the inverse cube root of the number of computational cells.

Which is given as

$$h = N^{-1/3} \tag{1}$$

Where N is the number of computational cells.

The observed orders of convergence were approximately 3.98 for Tco and 3.57 for LMTD. The fine-grid GCI values were estimated as 0.57% for T_{co} and 1.78% for LMTD. The GCI was estimated by

$$GCI_f = 1.25 \frac{\left|\phi_f - \phi_c\right|}{\left|\phi_f\right|\left(r^p - 1\right)} \times 100 \tag{2}$$

Where ϕ_f and ϕ_c are fine grid and coarse grids respectively, p is the observed order of convergence and r is the refinement ratio [27].

These relatively low GCI values indicate that the numerical discretization uncertainty associated with the finest mesh is small. Table 3.0 shows the summary of the GCI analysis.

Table 3.0 summary of the GCI analysis.

Parameter	Observed order p	Fine-grid change	Richardson extrapolation	Fine-grid GCI
Tco	3.98	0.727%	32.483 °C	0.57%
LMTD	3.57	1.916%	29.832 °C	1.78%

Consequently, the mesh containing 1,698,019 cells was selected for the subsequent simulations because it provides an appropriate balance between numerical accuracy and computational expense [28-30]. Fig. 3 shows the mesh independence and Grid convergence study based using LMTD and shell side outlet temperature as a check criteria.

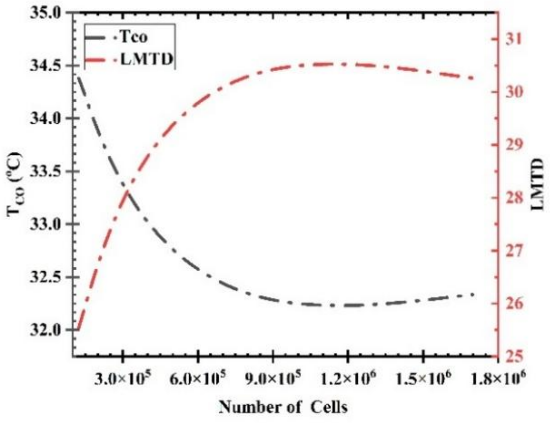


Fig. 3. Mesh independence and Grid convergence study based on LMTD and shell side outlet temperature.

2.3 Computational Methods

The fluid flow and heat-transfer fields were obtained by solving the steady conservation equations of mass, momentum and energy. Turbulent transport was represented using the classical k−ε empirical model. Heat conduction through the copper tube wall was solved simultaneously with convection in the fluid domains, thereby providing a conjugate heat-

transfer solution. The equations were discretized using the finite-volume method [31]. The Navier-Stokes equation, continuity, momentum, energy, and k and ε models were adopted for the turbulent flow prediction.

Continuity

$$\frac{\partial}{\partial x_i}\left(\rho u_i\right)=0 \tag{3}$$

Momentum:

$$\frac{\partial}{\partial x_i}\left(\rho u_i u_k\right)=\frac{\partial}{\partial x_i}\left(\mu\frac{\partial u_k}{\partial x_i}\right)-\frac{\partial P}{\partial x_i} \tag{4}$$

Energy:

$$\frac{\partial}{\partial x_i}\left(\rho u_i t\right)=\frac{\partial}{\partial x_i}\left(\frac{\partial t}{\partial x_i}\frac{k}{C_p}\right) \tag{5}$$

Turbulent kinetic energy:

$$\frac{\partial}{\partial x_i}\left(\rho u_i k\right)+\frac{\partial \rho k}{\partial t}=\frac{\partial}{\partial x_i}\left(\left(\mu+\frac{\mu_t}{\sigma_k}\right)\frac{\partial k}{\partial x_i}\right)+S_k \tag{6}$$

Turbulence dissipation energy:

$$\frac{\partial}{\partial x_i}\left(\rho u_i \varepsilon\right)+\frac{\partial \rho \varepsilon}{\partial t}=\frac{\partial}{\partial x_i}\left(\left(\mu+\frac{\mu_t}{\sigma_\varepsilon}\right)\frac{\partial \varepsilon}{\partial x_i}\right)+S_\varepsilon \tag{7}$$

The source term is given as S_k and S_ε where they are defined as

$$S_k=\tau_{ij}^R\frac{\partial u_i}{\partial x_i}-\rho\varepsilon+\mu_t P_B \tag{8}$$

and

$$S_\varepsilon=C_{\varepsilon 1}\frac{\varepsilon}{k}\left(f_1\tau_{ij}^R\frac{\partial u_i}{\partial x_i}+\mu_t C_B P_B\right)-C_{\varepsilon 2}f_2\frac{\rho\varepsilon^2}{k} \tag{9}$$

The turbulent generation that is due to buoyancy force P_B is represented as

$$P_B=-\frac{g_i}{\sigma_B}\frac{1}{\rho}\frac{\partial \rho}{x_i} \tag{10}$$

Where g_i is the component of gravitational acceleration in the direction of x_i the constants C_μ, $C_{\varepsilon 1}$, $C_{\varepsilon 2}$, σ_K ,and σ_ε are empirically defined. While in the flow simulation the following constant values, C_μ = 0.09, $C_{\varepsilon 1}$ = 1.44, $C_{\varepsilon 2}$ = 1.92, σ_k = 1, and σ_ε = 1.3, are adopted and used for this simulation [32, 33]. Where the Lewis number $L_e=1$ and

the constant σ_B and C_B are 0.9 and 1, respectively, when $P_B > 0$, then following the Boussinesq assumption, the Reynolds-stress tensor for Newtonian fluids has the following form

$$\tau_{ij}^{R} = \mu\left(\frac{\partial u_i}{\partial x_i} + \frac{\partial u_j}{\partial x_i} - \frac{2}{3}\delta_{ij}\frac{\partial u_k}{\partial x_k}\right) - \frac{2}{3}\delta_{ij}\rho k \tag{11}$$

Where δ_{ij} is the Kronecker delta function, which is equal to unity when $i = j$, and zero otherwise, μ is the dynamic viscosity coefficient, k is the turbulent kinetic energy, μ_t is the turbulent eddy viscosity coefficient derived from

$$\mu_t = f_\mu \frac{c_\mu \rho k^2}{\varepsilon} \tag{12}$$

Where f_μ is the turbulent viscosity factor, which is defined by the expression

$$f_\mu = \left(1 - e^{-0.0165 R_y}\right).\left(1 + \frac{20.5}{R_T}\right) \tag{13}$$

Where y is the distance from a point to the wall and Lam and Bremhorst's damping functions [34] could be estimated from the equation (12).

$$f_1 = 1 + \left(\frac{0.05}{f_\mu}\right)^3 \tag{14}$$

$$f_2 = 1 - \exp\left(-R_T^2\right) \tag{15}$$

Lam and Bremhorst's damping functions (f_μ, f_1 and f_2) modify the turbulence model near walls by reducing turbulent viscosity and turbulence kinetic energy while increasing dissipation at low Reynolds numbers [34]. When all damping functions equal unity that is (f_μ = 1, f_1 = 1 and f_2 = 1), the model reverts to the standard k–ε formulation. Fluid boundary layer behavior near solid walls is modeled by solving the Navier–Stokes equations with a two-equation k–ε turbulence model, while near-wall shear effects are accounted for using the Launder–Spalding wall-function approach [35].

When sufficient mesh resolution is available across the boundary layer (that is, ~10), laminar boundary layers are directly resolved using the Navier–Stokes equations. For turbulent boundary layers, SolidWorks Flow Simulation applies a Van Driest–based formulation (mixing length) to relate the dimensionless velocity, u^+ to the dimensionless wall distance, y^+ [36].

$$u^+ = \frac{u}{\sqrt{\frac{\tau_w}{\rho}}} \int_0^{y^+} \frac{2d\eta}{1 + \sqrt{1 + 4K^2\eta^2\left(1 - e^{\frac{\eta}{A_v}}\right)^2}} \tag{16}$$

Where K is the Karman constant (which is equal to 0.4504) and the Van Driest coefficient is A_v = 26.

Flow Simulation enables the numerical prediction of conjugate heat transfer between fluid and solid domains, accounting for interfacial energy exchange. Heat transfer within the fluid region is governed by the energy conservation equation, where the heat flux is defined in accordance with Fourier's law and convective transport mechanisms. In solid media, heat transfer is described by the anisotropic heat conduction equation, which accounts for direction-dependent thermal conductivity, which is given as

$$\frac{\partial \rho e}{\partial t} = \frac{\partial}{\partial x_i}\left(\lambda_i \frac{\partial T}{\partial x_i}\right) + Q_H \tag{17}$$

Where e is the specific internal energy, Q_H is the specific heat release (or absorption) per unit volume, while λ_i is the eigenvalue of the thermal conductivity tensor.
Energy exchange between the fluid and solid domains is evaluated through the diffusive heat flux normal to the solid–fluid interface, incorporating the solid surface temperature and, where applicable, the thermal characteristics of the adjacent fluid boundary layer.

The diffusive heat flux is expressed as

$$q_i = \left(\frac{\mu}{\Pr} + \frac{\mu_t}{\sigma_c} \right) \frac{\partial h}{\partial x_i} \qquad \text{i = 1.2.3} \qquad (18)$$

Where $\Pr$ is the Prandtl number, h is the thermal enthalpy, and σ_c = 0.9. For laminar flow the parameters μ_t and K are zero.

2.4 Boundary conditions

At the boundary condition, the no-slip condition was enforced on all solid internal surfaces, ensuring that the fluid velocity at the wall interface is zero relative to the boundary. The external shell wall is modeled with a zero heat flux boundary condition to simulate perfect insulation from the environment, while heat transfer between the internal water and the baffles is neglected to simplify the computational domain. A coupled heat transfer boundary condition is applied to the tube walls, allowing for the simultaneous calculation of thermal exchange between the shell-side and tube-side fluids. The system outlets for both the shell and tube sides are set to environmental conditions, with the overall environmental temperature fixed at 25°C to reflect ambient surroundings. Liquid water is utilized as the working fluid for both sides, entering the tube at a specified constant temperature. The adoption of standard wall functions indicates that the near-wall region was modeled using semi-empirical relations rather than fully resolving the viscous sublayer. In turbulent flows within shell-and-tube heat exchangers, the near-wall region exhibits steep velocity and temperature gradients that strongly influence pressure drop and heat transfer. Direct resolution of this region would require extremely fine meshes (with $y^+ \approx 1$), leading to prohibitive computational cost for industrial-scale geometries. Standard wall functions bridge the viscous sublayer and logarithmic region by imposing the logarithmic law of the wall. This approach assumes that the first computational node off the wall lies within the logarithmic layer, typically within the range of $30 \le y^+ \le 300$. The boundary conditions used in the CFD modelling is shown in Table 4.0

Table 4.0 boundary condition for the CFD modelling

Boundary conditions	**Description**
Tube wall Temperature	70 ºC
Shell wall Temperature	25 ºC
Shell and tube outlet Pressure	0 Pa
Shell and tube mass flow rate	0.25 kg/s and 0.1 kg/s respectively. Flow direction in the x direction.
Tube Material	Copper
Shell Material	Stainless steel
Working fluid	Water

Shell outer wall	Adiabatic wall; heat flux = 0 W/m^2, stationary wall, no slip condition.

2.5 Solver setup

The governing equations of mass, momentum, and energy conservation were discretized using the finite volume method (FVM). This choice is appropriate for heat exchanger simulations because FVM inherently enforces conservation over each control volume, which is essential for coupled thermohydraulic problems. The Semi-Implicit Method for Pressure-Linked Equations (SIMPLE) was employed to handle pressure–velocity coupling in the incompressible flow field. Because pressure does not have its own transport equation in incompressible flows, algorithms like SIMPLE are required to enforce mass conservation. The merits of SIMPLE are good numerical stability, moderate computational cost, and proven robustness for industrial flows. The Quadratic Upstream Interpolation for Convective Kinematics (QUICK) scheme was applied to discretize both convective and diffusive terms. QUICK is a higher-order upwind-biased scheme that provides third-order spatial accuracy on uniform grids. The advantage of this scheme is that it captures temperature gradients near tube walls and wake development behind tubes and shell-side mixing induced by baffles. The convergence criterion was taken as 10^{-4} for the flow equations and 10^{-8} for the energy equation. This choice reflects the stronger sensitivity of heat transfer predictions to residual errors in the energy equation. In heat exchanger simulations, small temperature errors can significantly affect calculated heat duty and overall HTC.

2.6 Examined quantities

2.6.1 Tube side pressure drop

Tube-side pressure drop is a fundamental hydraulic constraint in shell-and-tube heat exchanger design because it governs the required pumping power, operating cost, and allowable flow rate through the exchanger. While increasing flow velocity inside the tubes improves the tube-side heat transfer coefficient, it simultaneously increases frictional losses. Consequently, exchanger design is inherently a thermo-hydraulic optimization problem. Tube wall thickness enters this problem indirectly but importantly. Although thickness does not directly appear in the Darcy–Weisbach equation, it affects the tube inner diameter, which strongly controls velocity and frictional losses. In most industrial designs where the tube outer diameter is fixed by tube sheets and pitch requirements, increasing tube thickness reduces the flow area and can significantly increase tube-side pressure drop.

For N_p pass exchangers, the total tube-side pressure drop is typically expressed as:

$$\Delta P_t = \Delta P_{friction} + \Delta P_{\min or} \tag{19}$$

Where $\Delta P_{friction}$ is the distributed losses along the tube and $\Delta P_{\min or}$ is the entrance, exit, and return losses. The friction factor depends on the Reynolds number:

$$\mathrm{Re} = \frac{\rho V D_i}{\mu} \tag{20}$$

For laminar flow where ($\mathrm{Re} < 210$)

$$f = \frac{64}{\mathrm{Re}} \tag{21}$$

The turbulent flow equation is given as

$$3000 < \mathrm{Re} < 10^5 \tag{22}$$

Blasius correlation is expressed as

$$f = 0.316\,\mathrm{Re}^{-0.25}$$

The Darcy–Weisbach expression for frictional pressure drop for one pass is given as

$$P_f = f\frac{L_{eq}}{D_i}\frac{\rho V^2}{2} \tag{23}$$

Where f is the Darcy friction factor, L_{eq} is the equivalent tube length, V is the mean velocity in the tube, and ρ is the fluid density. The expression for the velocity for the tube per pass is given as

$$V = \frac{4\dot{m}_t}{\pi\rho N_t D_i^2} \tag{24}$$

Equation (20) shows the strong dependence of pressure drop on tube diameter. Where $\dot{m}_t$ is the tube-side mass flow rate, N_t is the number of tubes per pass. Substituting equation (24) into equation (23) gives the explicit diameter dependence.

$$\Delta P_t = \frac{8fN_pL}{\pi^2\rho N_t^2}\frac{\dot{m}_t^2}{D_i^5} \tag{25}$$

Minor losses are often estimated as

$$\Delta P_m = K\frac{\rho V^2}{2} \tag{26}$$

Where K is called the minor loss coefficient (or local loss coefficient). Which represents an additional pressure loss caused by flow disturbances, and they occur over short distances compared to friction losses along the tube length. For multipass shell-and-tube exchangers, the total minor losses are usually estimated as $\sum K \approx 1.5-2.5$ per pass. then

$$\Delta Pm \approx (1.5-2.5)^2\frac{\rho V^2}{2}\times N_p \tag{27}$$

The total pressure drop, including minor losses at the tube side, is therefore given as

$$\Delta P_t = (f\frac{L}{D_i} + \sum K)\frac{\rho V^2}{2} \tag{28}$$

2.6.2 Heat Transfer Coefficient

The overall HTC is commonly expressed in terms of the thermal resistances associated with convection, fouling, and conduction through the tube wall. For a cylindrical tube based on the outer surface area, the overall HTC can be written as

$$\frac{1}{U_o} = \frac{1}{h_i}\frac{D_o}{D_i} + R_{f,i}\frac{D_o}{D_i} + \frac{D_o ln(D_o/D_i)}{2k_w} + R_{f,o} + \frac{1}{h_o} \tag{29}$$

Where h_i and h_o are the tube-side and shell-side HTCs respectively, $R_{f,i}$ and $R_{f,o}$ are the fouling resistances, D_o and D_i are the outer and inner tube diameters, respectively; and k_w is the thermal conductivity of the tube material.

$$\frac{D_o \ln\left(\frac{D_o}{D_i}\right)}{2K_w} \tag{30}$$

The term represents the thermal resistance of the tube wall. This term directly depends on the tube thickness. The relationship between tube thickness and the tube diameters is given by

$$t = \frac{D_o - D_i}{2} \tag{31}$$

or equivalently

$$D_i = D_o - 2t \tag{32}$$

Substituting this expression into the wall resistance term shows that increasing the tube thickness increases the logarithmic conduction resistance.

For thin-walled tubes where the thickness is small compared with the tube diameter, the logarithmic term can be approximated using the thin-wall assumption, giving as

$$R_w = \frac{t}{k_w} \tag{33}$$

2.6.3 Thermal stress

Thermal stress in shell-and-tube heat exchangers arises when temperature gradients develop within the tube wall and when thermal expansion is constrained by surrounding structures such as tube sheets, baffles, and supports.

Thermal stress can be approximated by

$$\sigma_t = \frac{E\alpha\Delta T}{1-\upsilon} \tag{34}$$

Where σ_t is the thermal stress, E is the young modulus, α the coefficient of thermal expansion, υ Poisson's ratio, and ΔT the temperature difference across the walls.

3.0 Results and discussions

3.1 Effect of tube thickness on the HTC

As depicted in Fig. 4.0, the effect of tube thickness on the HTC. As the tube wall becomes thicker or increases from 0.5 mm to 2.0 mm, heat would have to travel through a longer conduction path, resulting in a larger temperature drop across the wall. Consequently, the overall thermal resistance of the exchanger increases and the overall HTC decreases, as shown in Fig. 5.0.

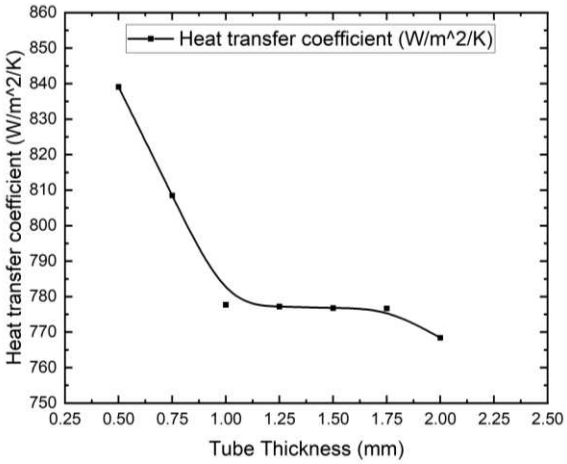


Fig. 4. the effect of tube thickness on the HTC.

Fig. 4.0 depicts that the HTC at 0.5 mm thickness was 821.2 W/m²/K and at 2.0 mm thickness 682.902 W/m²/K respectively. Thus, increasing tube wall thickness increases the conductive resistance of the tube wall, thereby reducing the overall HTC of the shell-and-tube heat exchanger. Although this negatively affects thermal performance, thicker tubes enhance mechanical strength and durability, making the selection of tube thickness a critical compromise between thermal efficiency and structural reliability in heat exchanger design. It is clear that the tube wall thickness influences the overall HTC in a shell-and-tube heat exchanger mainly through the thermal resistance of the tube wall. Heat must pass through the tube wall from the hot fluid to the cold fluid, and the thickness of this wall determines how easily heat can conduct through it.

3.2 Effect of tube thickness on the tube side pressure drop.

Fig. 5 illustrates the effect of tube-wall thickness on the tube-side pressure drop of the shell-and-tube heat exchanger. As the tube-wall thickness increased from 0.50 to 2.00 mm, while the tube outside diameter was maintained constant at 9.5 mm, the tube-side pressure drop increased substantially from 65.3 Pa to 3.35 kPa. This represents an approximately 51.3-fold increase in pressure drop, demonstrating the strong and nonlinear influence of tube-wall thickness on the hydraulic performance of the exchanger. The increase is primarily associated with the reduction in tube internal diameter, which decreased from 8.5 mm at a wall thickness of 0.50 mm to 5.5 mm at 2.00 mm. It could also as a resulting of keeping the total tube-side mass flow rate constant, therefore, the reduction in flow area caused the fluid velocity within each tube to increase substantially. Consequently, the hydraulic resistance increased as the tube diameter decreased. For fully developed laminar flow at constant mass flow rate, the frictional component of pressure loss has an approximate inverse fifth-power dependence on internal diameter. This indicates that, in addition to the reduction in internal diameter, this might be due to the hydraulic effects, including changes in Reynolds number, frictional behaviour, entrance and exit losses, flow acceleration and deceleration, and the additional losses associated with the two-pass tube arrangement. The progressively increasing pressure drop therefore results from the combined effect of decreasing flow area and increasing hydraulic resistance as the tube wall becomes thicker. These findings are in line with the work of Krisdiyanto et al. [25].

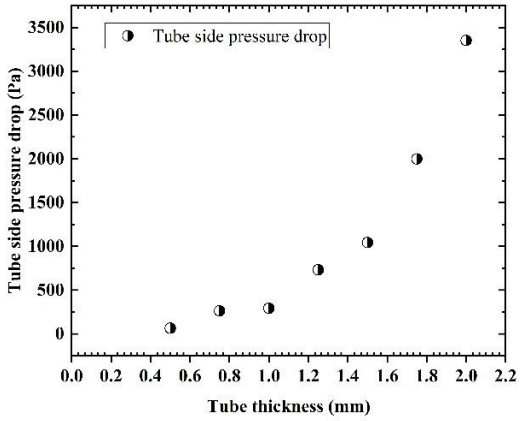


Fig. 5. the effect of tube thickness on the on the tube side pressure drop.

3.3 Temperature distribution along the shell side

The temperature-flow trajectories for the seven tube-wall thicknesses, presented in Fig.s 6(a–g), demonstrate the progressive thermal interaction between the hot tube-side and cold shell-side fluids under parallel-flow conditions. The hot fluid enters the tube bundle at approximately 70°C, while the shell-side fluid enters at approximately 25°C. As both streams proceed in the same axial direction, the local temperature difference decreases progressively along the exchanger length as heat is transferred from the tube-side fluid to the shell-side fluid. The repeated deflection of the trajectories around the baffles indicates the influence of the baffled shell-side flow on thermal mixing and heat exchange. With increasing tube-wall thickness from 0.50 to 2.00 mm, the tube-side outlet temperature increased progressively from 43.54 to 50.60°C, while the shell-side outlet temperature decreased from 35.18 to 33.80°C. This behaviour indicates a progressive reduction in the net heat transferred between the two streams as the tube wall becomes thicker. The reduction is associated with the increased tube-wall conduction resistance resulting from the reduced tube internal diameter, together with changes in tube-side flow characteristics. The temperature trajectories therefore demonstrate that tube-wall thickness has a measurable influence on the thermal development of both streams, with thinner tubes providing greater cooling of the hot fluid and greater heating of the cold fluid.

For the 0.5 mm wall as shown in Fig. 6(a). It can be seen that the fluid temperature at 25 ^{o}C indicated by the blue colour progressively receives heat from the hot tube as the fluid is exiting the shell side at approximately 35^{o}C. Similarly, a larger portion of the tube-side flow loses heat, indicating enhanced heat transfer due to the relatively low thermal resistance of the thin tube wall. As seen in Fig. 6(a) at 0.5 mm tube thickness, it was observed that the tube-side fluid experience loss of heat from the tube side to the shell fluid. The temperature contours show a relatively extensive region of red-to-light green temperature as the fluid moves through the tube bundle and existing the tube

side at approximately 44 ºC. This indicates relatively effective heat transfer from the hot tube-side fluid to the shell-side fluid because of the thin wall and low conduction resistance.

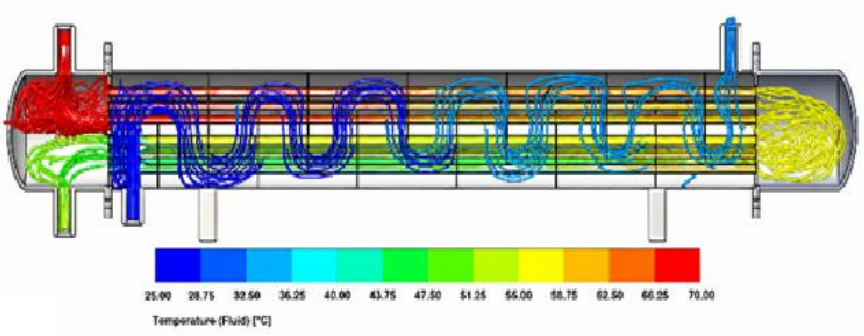
Fig. 6 (b) show the contour plot for 0.75 mm tube thickness. It is seen that the temperature distribution remains similar to Fig. 6(a), but the extent of the higher-temperature region is slightly reduced. The shell fluid is still effectively heated, although the increase in wall thickness introduces additional thermal resistance. It can be seen that the hot fluid entered the tube side at 70 ºC and exited the tube side at approximately 45 ºC. At the shell side. the cold fluid received heat and the temperature at the exit of the shell was increase to about 34.97 ºC. From the contour plot in Fig. 6(b), it can be seen that the shell side recorded a region of blue to light green temperature as the fluid flowed through the shell. While the tube side recorded a temperature region from red light green section of the temperature profile.

For the 1.0 mm tube thickness as depicts in Fig. 6(c), it can be seen that a gradual reduction in tube-side heating becomes evident. More of the tube-side flow remains in the blue/cyan temperature range, indicating that the shell fluid receives slightly less thermal energy than in the thinner-wall cases.

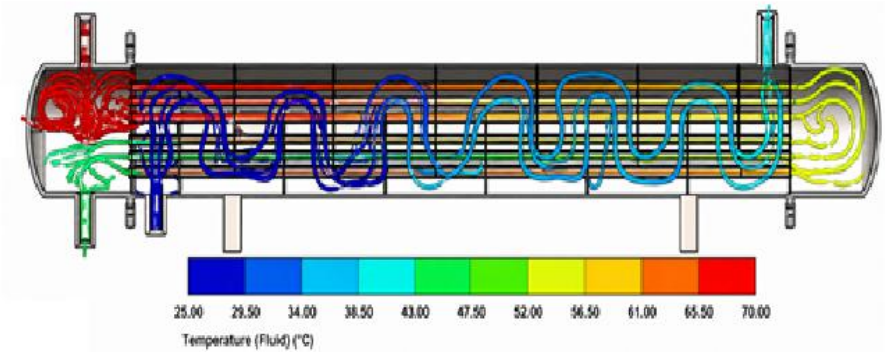
In Fig. 6(d), the temperature field becomes comparatively cooler over much of the shell-side flow path. The higher-temperature region is more concentrated toward the downstream portion of the exchanger, suggesting reduced heat transfer through the thicker tube wall. However, Fig. 6(e) displayed at the 1.5 mm tube thickness shell-side temperature distribution shows a further reduction in the extent of the warmer regions. A significant portion of the shell-side fluid remains at relatively low temperatures, demonstrating the increasing thermal resistance associated with the thicker wall. In Fig. 6(f) the effect becomes more pronounced where the shell-side fluid is heated less effectively along the exchanger length, with the warmer temperatures concentrated closer to the shell-side outlet region.

At 2 mm tube thickness as depicts in Fig. 6(g), the thickest tube wall produces the least extensive heating of the shell-side fluid. The contour is dominated by the lower-temperature colours over much of the flow path, while the higher temperatures occur mainly toward the outlet. This indicates the lowest thermal effectiveness among the seven configurations.

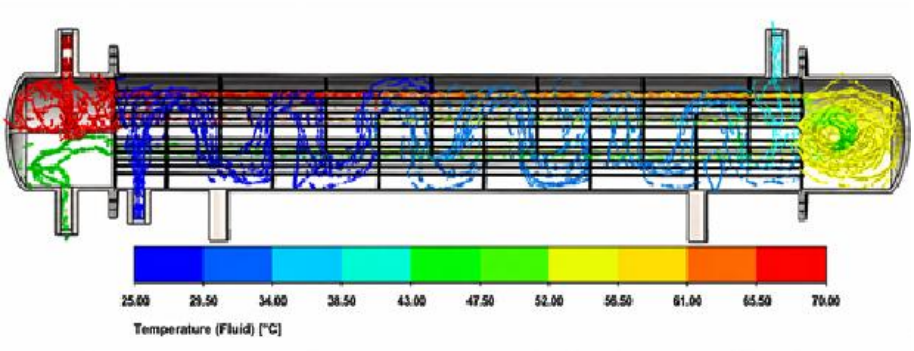
Overall, the contours confirm that increasing tube-wall thickness adversely affects the thermal performance of the exchanger, with the 2.0 mm configuration exhibiting the least effective shell-side heating.



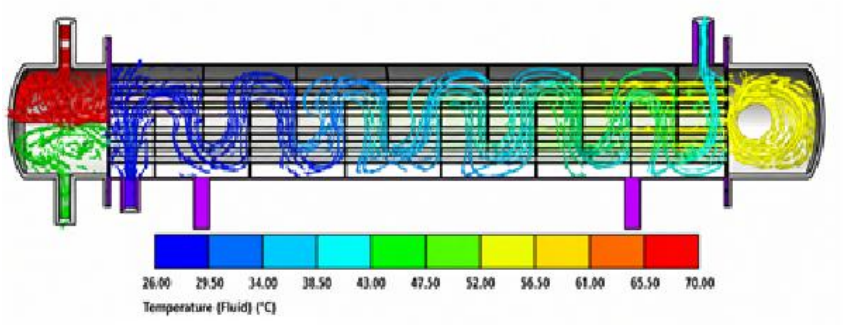
(a)



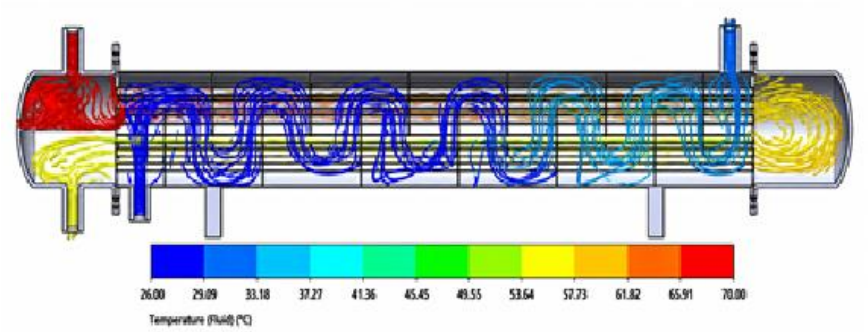
(b)


25.00 29.50 34.00 38.50 43.00 47.50 52.00 56.50 61.00 65.50 70.00
Temperature (Fluid) [°C]

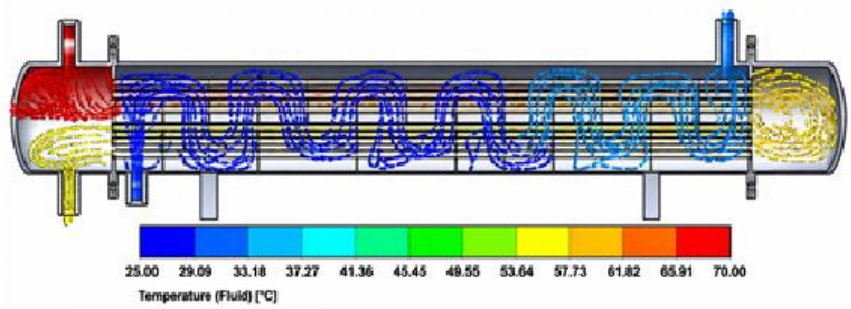
(c)


26.00 29.50 34.00 38.50 43.00 47.50 52.00 56.50 61.00 65.50 70.00
Temperature (Fluid) [°C]

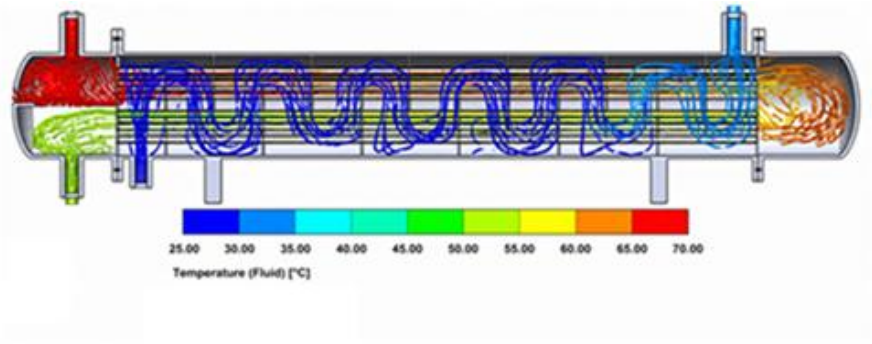
(d)


26.00 29.09 33.18 37.27 41.36 45.45 49.55 53.64 57.73 61.82 65.91 70.00
Temperature (Fluid) [°C]

(e)


25.00 29.09 33.18 37.27 41.36 45.45 49.55 53.64 57.73 61.82 65.91 70.00
Temperature (Fluid) [°C]

(f)

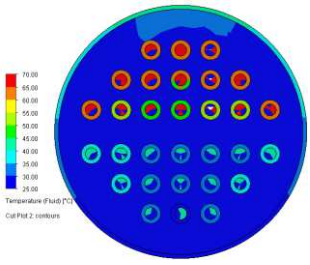
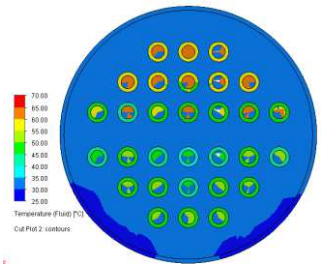
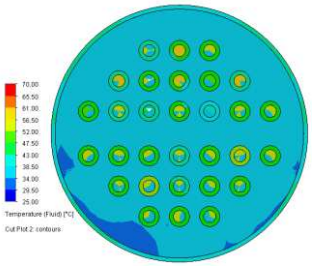
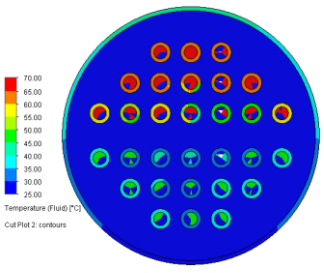
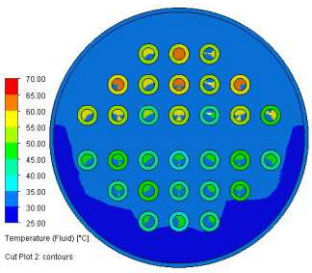
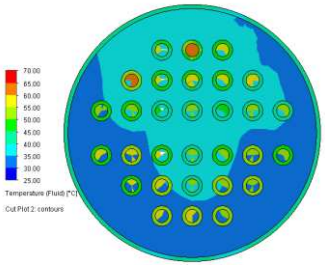


(g)

Fig. 6. the contour of temperature distribution (axial thermal behavior) in the shell section with tube thickness (a) 0.5 mm (b) 0.75 mm (c) 1.0 mm (d) 1.25 mm (e) 1.5 mm (f) 1.75 mm and (g) 2.0 mm.

3.4 Tube wall temperature gradient

The temperature contours at various radial sections of the shell is illustrated in Fig. 7. These view represent temperature gradient on the tube taken from the radial section: 5 mm from the tube inlet, the midsection is at 400 mm, and 795 mm is toward the tube exit. The temperature distribution results depicted in Fig. 7 reveal that increasing tube wall thickness significantly alters both radial and axial thermal behavior along the exchanger length. At approximately 5 mm from the inlet region, it is seen that the thermal driving force is highest, thicker tubes exhibit a pronounced increase in radial temperature gradient due to enhanced conduction resistance. In the fully developed region at the center of the pipe, about 400 mm , the temperature field is increasingly dominated by the wall, with a larger fraction of the temperature drop occurring across the tube thickness rather than within the fluid. Towards the outlet at about 795 mm, the effect of tube thickness on fluid temperature diminishes as the temperature difference between the fluids decreases,although substantial gradients persist within the tube wall. Overall, increasing tube thickness shifts the thermal resistance from the fluid to the solid domain, resulting in reduced heat transfer effectiveness and increased thermal gradients within the wall.

	(a)	(b)	(c)
2.0mm			
1.75 mm			

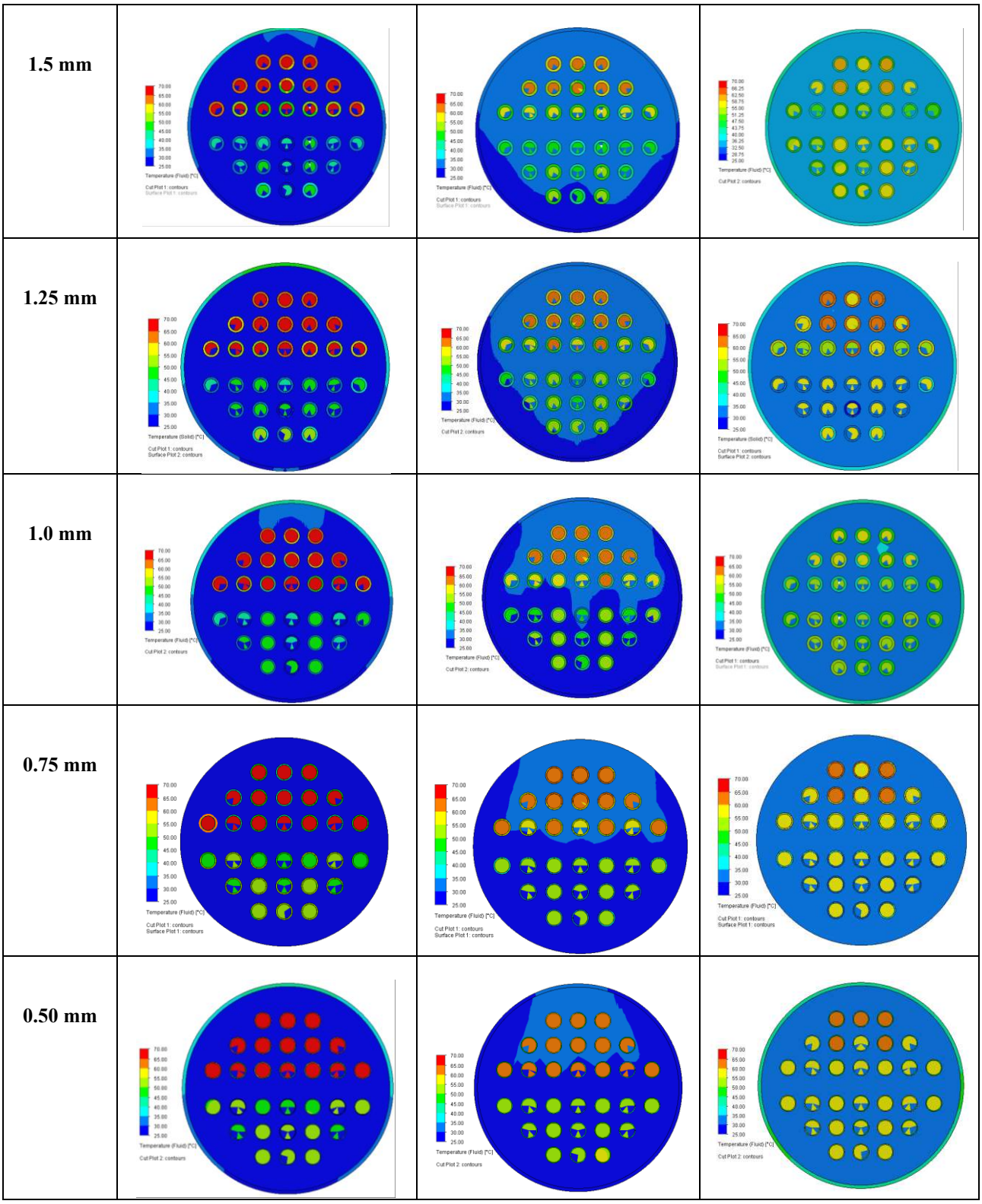
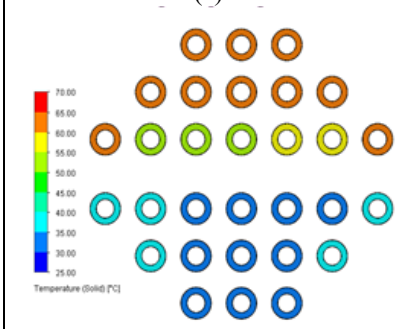
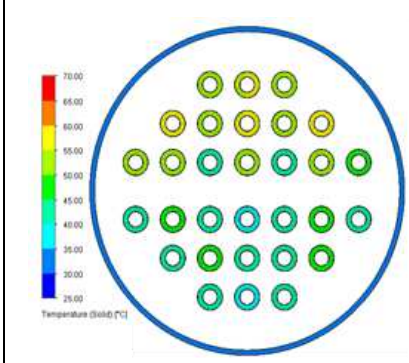
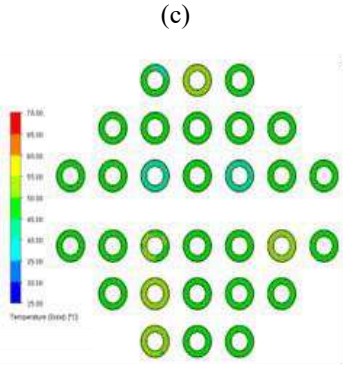
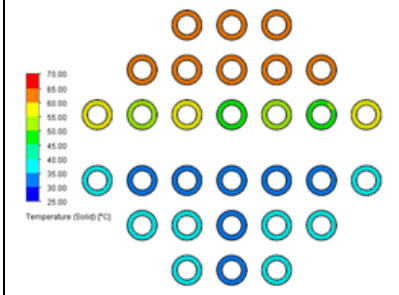
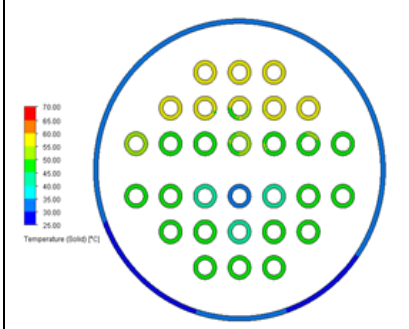
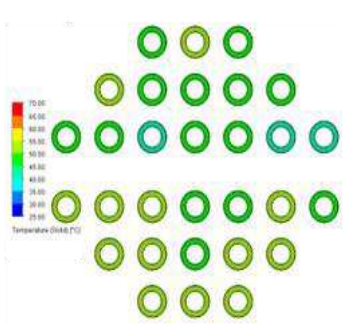
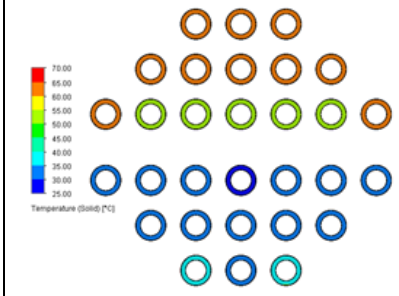
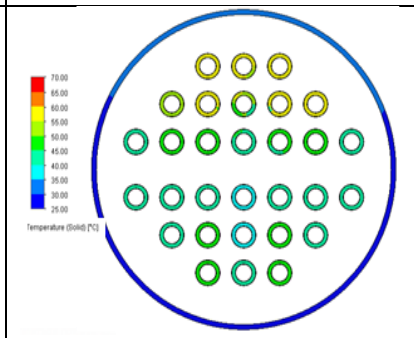
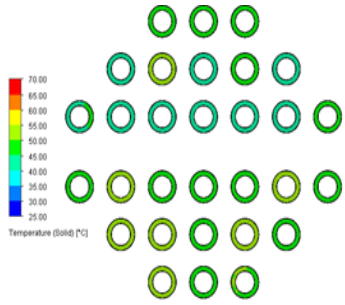
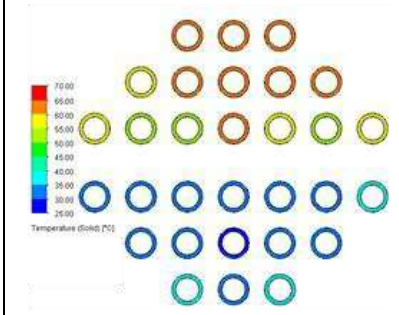
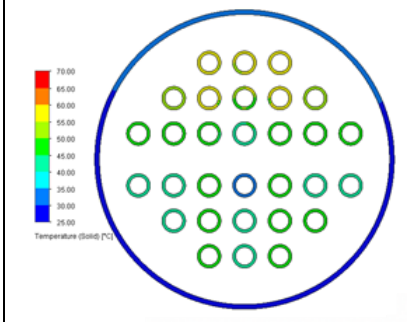
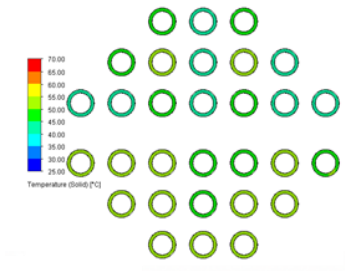


Fig. 7. the temperature profiles at the cross section of the STHE at (a) 5 mm from the inlet, (b) 400 mm at the center of the shell, and (c) at 795 mm from the inlet of the tube.

2.0mm	(a) 	(b) 	(c) 
1.75 mm			
1.5mm			
1.25mm			

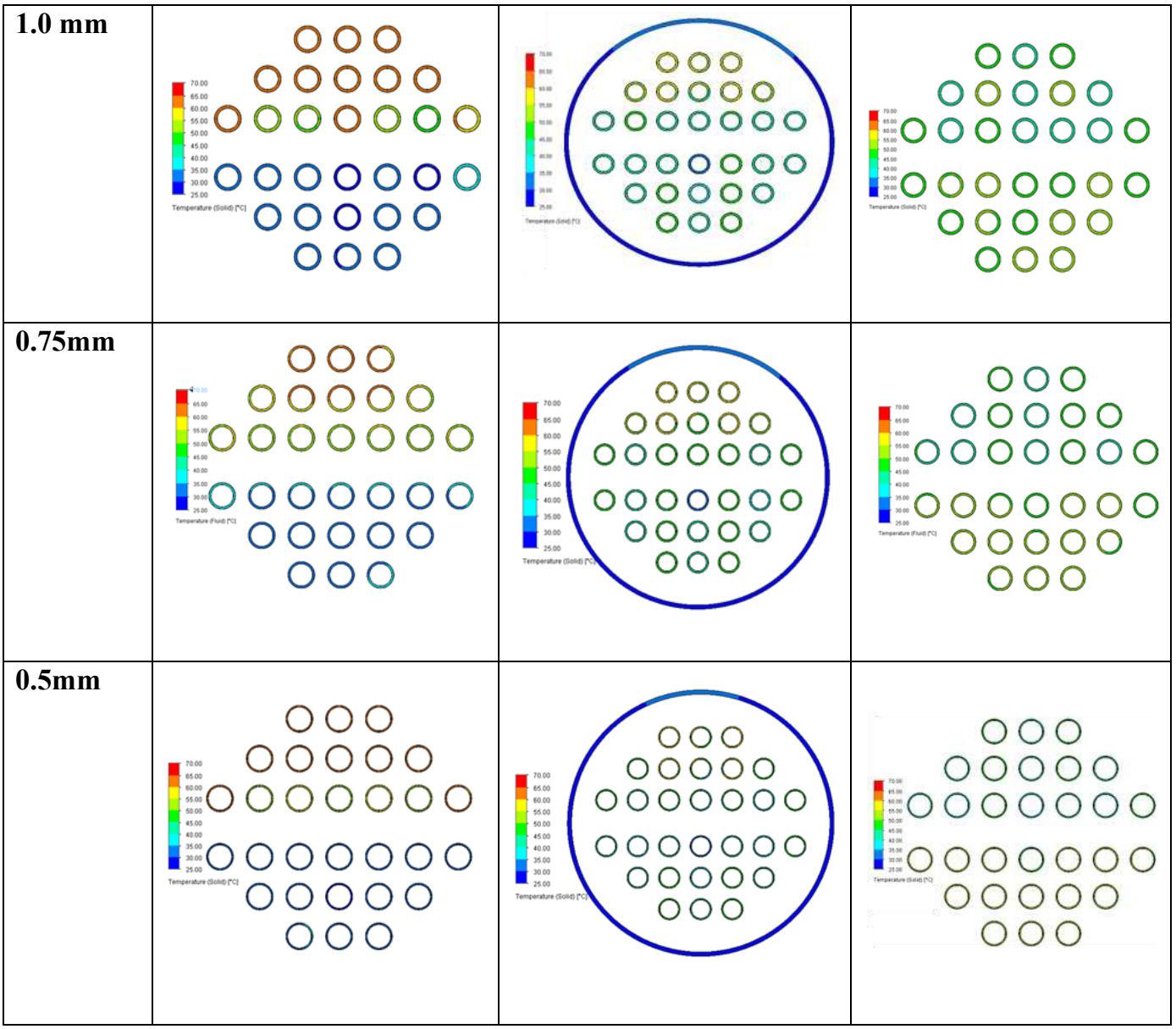


Fig. 8. the temperature profiles at the cross section of the tubes at (a) 5 mm from the inlet, (b) 400 mm at the center of the shell, and (c) at 795 mm from the inlet of the tube.

Fig. 8 presents the temperature profiles across the tube bundle at three axial locations, namely 5 mm from the tube inlet, 400 mm at the centre of the shell, and 795 mm from the tube inlet, for tube-wall thicknesses ranging from 0.50 to 2.00 mm. The colour contours reveal a pronounced cross-sectional temperature non-uniformity close to the inlet. At 5 mm, the upper region of the tube bundle is predominantly characterized by orange/brown colours, corresponding to the higher-temperature region, whereas the central tubes exhibit predominantly green colours and the lower tubes contain blue/cyan colours representing relatively lower temperatures. This spatial variation indicates that the tubes are exposed to different local thermal environments as a result of the non-uniform shell-side flow and mixing around the tube bundle. As the flow progresses to the mid-section at 400 mm, the temperature distribution becomes more homogeneous, with green becoming the dominant colour and only localized yellow-green and cyan regions remaining. Near the outlet at 795 mm, the tube bundle is predominantly green, indicating further thermal development and a reduction in the cross-sectional temperature gradient. The progression from the strongly stratified temperature field near the inlet to a more uniform distribution downstream demonstrates the cumulative effect of heat transfer and fluid mixing along the exchanger length. Furthermore, increasing tube-wall thickness modifies the thermal development of

the tube bundle. The thicker tubes generally retain higher temperatures toward the outlet, consistent with the increase in the predicted tube-side outlet temperature from 43.54°C for the 0.50-mm tube to 50.60°C for the 2.00 mm tube. The results therefore indicate that tube-wall thickness influences not only the outlet temperature but also the spatial distribution and thermal development of the tube bundle along the exchanger.

3.6 Effect of thickness on the thermal stress/Von Mises stress distribution

Fig. 9 illustrates the variation of thermal stress with tube wall thickness. It is observed that thermal stress decreases progressively as the tube thickness increases from 0.5 mm to 2.0 mm in line with Krisdiyanto et al. work [27]. This behavior is attributed to the increased structural stiffness of thicker tubes, which reduces deformation under thermal loading. Although thicker tubes exhibit higher thermal resistance and larger temperature gradients, the enhanced rigidity allows for better distribution of thermal stresses, thereby lowering the peak stress values. The trend also indicates diminishing reduction in stress at higher thickness values, suggesting that beyond a certain thickness, further increases provide limited structural benefit.

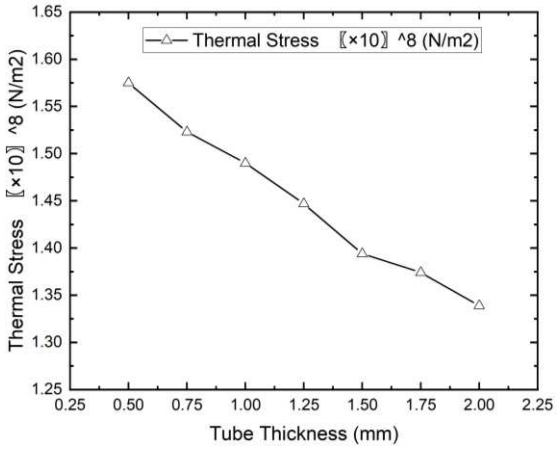


Fig. 9. the effect of tube thickness on the thermal stress.

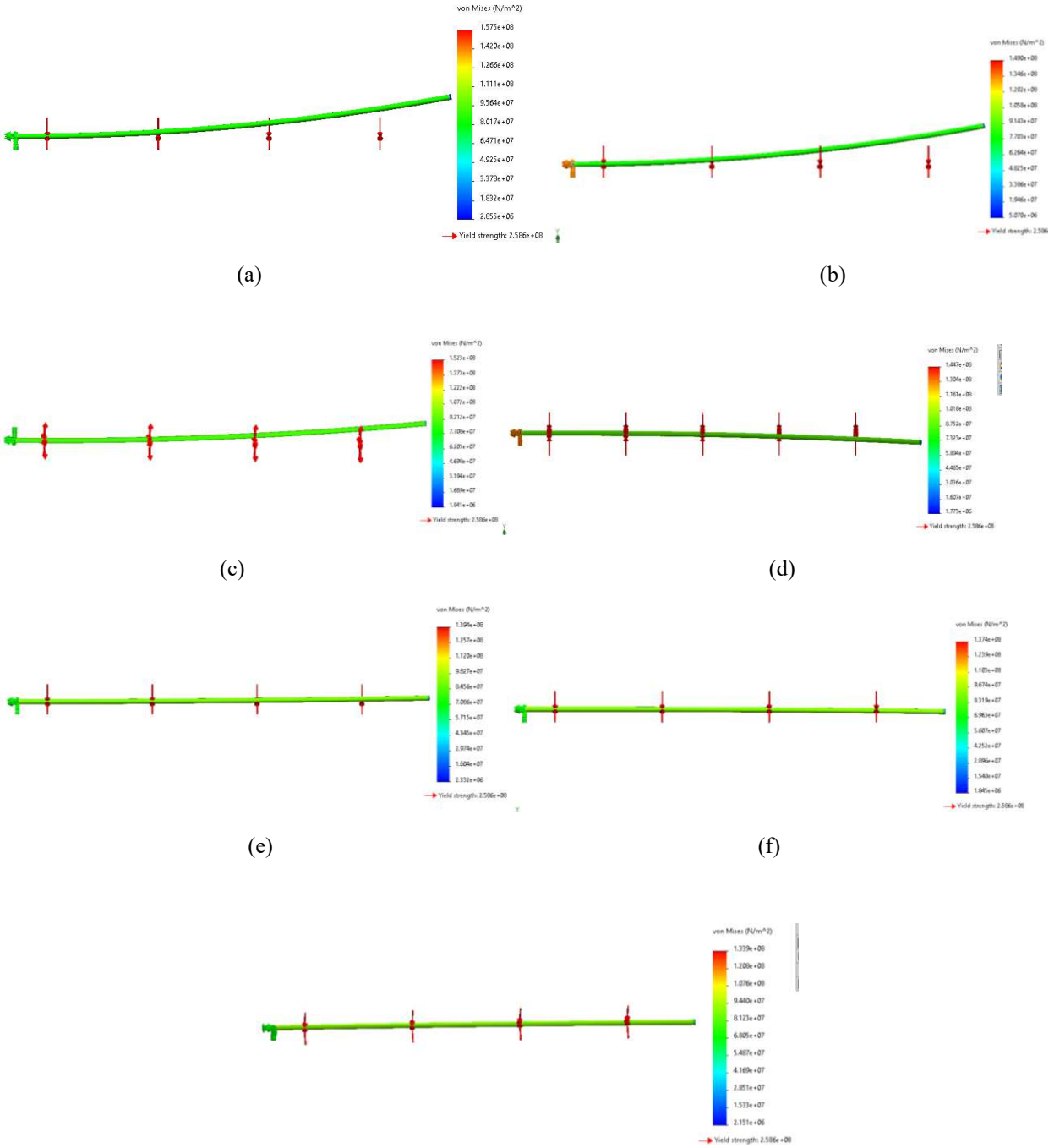
The effect of tube wall thickness on the Von Mises stress distribution in a shell-and-tube heat exchanger is fundamentally governed by the development of thermal stress within the tube material. Thermal stress arises due to temperature gradients across the tube wall and the restriction of thermal expansion imposed by structural constraints such as tube sheets and supports. As the tube thickness increases, both the magnitude of the temperature gradient and the level of constraint-induced stress increases, thereby directly influencing the Von Mises stress distribution. Fig. 10. depicts the contour of thermal stresses under varying tube thickness. Fig. 10(a) shows the contour of Von Mises stress distribution on the tube length with a tube thickness of 0.5 mm. At the smallest tube thickness, the thermal stress distribution is relatively low and uniform along the tube length. The small wall thickness results in a minimal temperature gradient across the wall, allowing the tube to expand more freely with limited stress concentration. The thinnest tube experiences the highest von Mises stress, reaching approximately 1.575×10^8 Pa**.** The stress is concentrated mainly around the constrained/support regions and near the tube inlet.

Fig. 10(b) shows the contour plot at 0.75 mm thickness; here a slight increase in thermal stress is observed compared to 0.5 mm. The stress distribution remains fairly uniform, although small variations begin to appear near the inlet region due to the developing temperature gradient. For thin tubes in the range of 0.5–0.75 mm, the thermal resistance of the wall is relatively low, resulting in a small temperature difference across the tube thickness. This leads to a more uniform temperature distribution between the inner and outer surfaces.

As a result, thermal stresses are lower because the tube material experiences minimal temperature-induced strain. Additionally, the reduced wall thickness allows the tube to expand more freely under thermal loading, thereby minimizing constraint effects and further reducing the development of thermal stress. In Fig. 10(c) at 1.0 mm thickness, the thermal stress increases further as the wall thickness increases. The temperature gradient across the tube wall becomes more pronounced, leading to noticeable stress variation along the tube, particularly near the inlet and constrained regions. At 1.25 mm thickness, the contours plot shows that at this thickness, the stress distribution becomes more non-uniform. Localized stress concentrations begin to develop, especially near the tube inlet and tube-sheet interface, as a result of increased thermal resistance and reduced structural flexibility.

Then a significant increase in thermal stress is observed in Fig. 10(e). The larger temperature difference across the wall leads to higher thermal strain mismatch, with clear stress concentration zones forming along the tube, particularly

near the inlet and support regions. At 1.75 mm tube thickness, Fig. 10 (f) shows that the thermal stress continues to increase and becomes more localized. The tube exhibits higher stiffness, restricting thermal expansion and causing pronounced stress gradients across the wall and along the axial direction. In Fig. 10 (g), shows the tube thickness on von mises at 2 mm thickness. The thickest tube exhibits the lowest maximum von Mises stress, approximately 1.34×10^8 Pa, indicating the greatest resistance to the thermally induced stresses among the seven cases. Fig. 10 (a)–(g) demonstrate that increasing tube-wall thickness progressively reduces the magnitude of von Mises stress and produces a more uniform stress distribution along the tube. The maximum stress decreases from approximately 1.575×10^8 Pa at 0.5 mm to about 1.34×10^8 Pa at 2.0 mm, indicating improved structural resistance with increasing wall thickness.



(a) (b)

(c) (d)

(e) (f)

(g)

Fig. 10. the contour of Von Mises stress distribution on tubes at (a) 0.5 mm, (b) 0.75 mm, (c) 1.0 mm, (d) 1.25 mm, (e) 1.5 mm, (f) 1.75 mm, and (g) 2.0 mm.

3.7 Thermal hydraulic – structural trade off

The effect of tube-wall thickness on shell-and-tube heat exchanger performance cannot be assessed using heat-transfer performance alone, because any improvement in thermal performance must be considered alongside the associated hydraulic penalty and structural response. In the present study, increasing the tube-wall thickness from 0.5 to 2.0 mm produced simultaneous changes in the overall heat-transfer coefficient, tube-side pressure drop, and thermal stress. Therefore, the selection of an appropriate tube-wall thickness represents a multi-criteria design problem involving a compromise between thermal efficiency, pumping-power requirement, and structural reliability. From the thermal perspective, increasing the tube-wall thickness introduces a longer conduction path between the shell-side and tube-side fluids. The corresponding cylindrical-wall thermal resistance increases with wall thickness, reducing the overall heat-transfer coefficient. The present numerical results show a reduction in the heat-transfer coefficient from approximately 821.2 W/m²K at 0.5 mm to 682.9 W/m²K at 2.0 mm. This represents a reduction of approximately 16.8%, indicating that excessive wall thickness can adversely affect the thermal effectiveness of the exchanger. The hydraulic response is even more sensitive to wall thickness when the tube outer diameter is maintained constant. Increasing the wall thickness reduces the internal tube diameter, thereby reducing the available flow area. For a prescribed mass flow rate, this reduction in flow area increases the mean fluid velocity and consequently increases frictional losses. In the present study, the tube-side pressure drop increased from approximately 65.3 Pa at the lower wall thickness to about 3.35 kPa at the highest thickness investigated. Thus, although thicker tubes may provide greater mechanical robustness, they impose a substantial hydraulic penalty and can increase the pumping power required to maintain the specified flow rate.

The structural response introduces the third component of the trade-off. A tube with a relatively thin wall contains less material to resist pressure loading, thermal expansion and deformation, and may therefore be more susceptible to mechanical instability, vibration, and fatigue under demanding operating conditions. Conversely, increasing the wall thickness generally provides greater cross-sectional stiffness and resistance to mechanical damage. This work identifies this structural advantage as one of the principal reasons for considering thicker tube walls despite their adverse thermal and hydraulic effects.

Consequently, neither the minimum nor the maximum wall thickness can automatically be considered the optimum design. The 0.5 mm tube provides the highest heat-transfer coefficient and the lowest pressure drop among the investigated cases, but the designer must ensure that its structural response remains within acceptable stress, deformation, fatigue and pressure-safety limits. At the other extreme, the 2.0 mm tube provides a substantially thicker structural section, but its thermal advantage is limited while its hydraulic penalty is considerable. An important observation from the present results is that the hydraulic penalty associated with increasing wall thickness is considerably more pronounced than the reduction in heat-transfer coefficient. The heat-transfer coefficient decreases by approximately 16.8% between the 0.5 and 2.0 mm cases, whereas the pressure drop increases from 65.3 Pa to approximately 3352 Pa, corresponding to an increase of approximately 50.33%. This demonstrates that tube-wall thickness should not be selected solely from a thermal-resistance perspective. In particular, when the outer tube diameter is fixed, relatively small increases in wall thickness can produce disproportionately large hydraulic penalties because of the reduction in internal flow diameter.

3.0 Conclusion

This study numerically investigated the effect of tube-wall thickness on the thermohydraulic and structural performance of a shell-and-tube heat exchanger using CFD and structural analysis. Seven tube-wall thicknesses ranging from 0.5 to 2.0 mm were evaluated under identical operating conditions. The results demonstrated that the hot-fluid tube outlet temperature increases from 43.54 to 50.60°C, indicating reduced heat removal from the hot stream while the cold fluid outlet temperature reduces from 35.18 °C to 33.80 °C. Increasing wall thickness reduces thermal performance because of the increased conduction resistance of the tube wall but causes a 51.3-fold increase in tube-side pressure drop from 65.3 Pa to approximately 3.35 kPa. This effect might be that the outer diameter of the tube pipe is fixed while varying the internal diameter and also could be due to the high reduction in internal pipe diameter increased the fluid velocity and frictional losses thereby causing an exponential effect on the tube side pressure drop. An overall reduction in heat-transfer coefficient from approximately 821.2 to 682.9 W/m²K amounting to approximately 16.8%. However, the maximum von Mises stress decreased from approximately 1.575×10^8 Pa at 0.5 mm wall thickness to 1.34×10^8 Pa at 2.0 mm, representing an overall reduction of approximately 15%. The temperature contours further showed that thicker tube walls produce larger radial temperature gradients and reduce the thermal driving force available for fluid-to-structure heat transfer. The structural analysis also demonstrated that

wall thickness influences the distribution of thermal stress, particularly around constrained regions such as the tube-sheet and inlet areas.
Overall, the modelling confirms a clear thermal–hydraulic–structural trade-off: thinner walls of about 5 mm favour heat transfer and reduce pressure drop, whereas thicker walls provide greater structural robustness but impose thermal and hydraulic penalties. Therefore, tube-wall thickness should be selected based on a balance between heat-transfer requirements, allowable pressure drop, and structural safety rather than on any single performance parameter. The findings highlight a fundamental trade-off between thermal efficiency, hydraulic performance, and mechanical strength and the CFD structural modelling approach provides a useful basis for optimizing tube-wall thickness and can be extended through experimental validation and multi-objective optimization to identify the most appropriate design for specific operating conditions.

3.1 Future work

Based on the findings and scope of the present investigation, the following areas are recommended for future research:

1. Future work should be carried out to experimentally validate the predicted heat-transfer performance, temperature distribution and pressure drop for different tube wall thicknesses. The analysis should also be extended to transient thermal loading and fatigue-life assessment to provide a more comprehensive evaluation of structural integrity.
2. Future studies should investigate the simultaneous optimisation of tube wall thickness, tube number, tube length, baffle spacing and other geometric parameters, with heat-transfer performance, pressure drop, thermal stress, material usage and pumping power considered as competing objectives. Multi-objective algorithms such as NSGA-II can be employed to identify Pareto-optimal designs.
3. Machine-learning surrogate models can be developed from validated CFD results to rapidly predict heat-transfer coefficient, pressure drop and thermal stress. These models can subsequently be integrated with evolutionary optimisation techniques to develop a computationally efficient design framework for selecting cost-effective STHE configurations while satisfying thermal, hydraulic and structural constraints.

4.0 Declarations

4.1Availability of data and materials

Data used in the modeling was generated from literature

4.2 Competing interests

The authors certify that they have no known financial or personal interests that could be interpreted as influencing or compromising the integrity of the work presented in this paper. The authors acknowledge the existence of the following financial interests/personal relationships that may be perceived as potential competing interests.

4.3 Funding

Thanks to the Federal Government of Nigeria, through the office of the Tertiary Education Trust Fund (TETFund), for sponsoring this research through the Institutional-Based Research (IBR) grant

4.4 Data availability

The datasets generated during and/or analysed during the current study are available from the corresponding author on reasonable request. All data supporting the findings of this study are included within the article and its supplementary information files where applicable

4.5 Authors' contributions

Nyong, Oku Ekpenyong. (Conceptualization; formal analysis; visualization; software; writing-original draft; validation; supervision).
Udeme, Victor Akpan (investigation; methodology; data curation; writing – review & editing; resources)
Ana, Raymond. (writing review and editing; project administration)
Ogban-Ekpe, Gideon .Adonokpem (formal analysis; project administration)
Eyo, Ukpabio Ekpenyong (project administration)
Obi, Edward Asu (project administration)

4.6 Acknowledgements

A final thanks to the Department of Mechanical Engineering, the University of Cross River State, where the research work was carried out.

References

[1] Krisdiyanto K, Adi RK, Sudarisman S, Hamdan SB. An analysis of tube thickness effect on shell and tube heat exchanger. Eastern-European Journal of Enterprise Technologies. 2021;1:25-35 DOI: 10.15587/1729-4061.2021.225334.

[2] Marzouk SA, Abou Al-Sood MM, El-Said EMS, Younes MM, El-Fakharany MK. A comprehensive review of methods of heat transfer enhancement in shell and tube heat exchangers. Journal of Thermal Analysis and Calorimetry. 2023;148:7539-78 DOI: 10.1007/s10973-023-12265-3.

[3] Dogan B. Numerical investigation of conjugate heat transfer in circular pipes considering wall thickness, material conductivity, and external convection. Results in Engineering. 2026;29:109236 DOI: 10.1016/j.rineng.2026.109236.

[4] Rahman MA. Enhancing Reliability in Shell and Tube Heat Exchangers: Establishing Plugging Criteria for Tube Wall Loss and Estimating Remaining Useful Life. Journal of Failure Analysis and Prevention. 2024;24:1083-95 DOI: 10.1007/s11668-024-01934-6.

[5] Abubakar M, Siddique M, Rasheed S, Khan M. Computational Fluid Dynamics and Thermal Performance Optimization of a Shell and Tube Heat Exchanger. 4th International Conference on Key Enabling Technologies (KEYTECH 2024 …, 2024. 2024.

[6] Xiao J, Duan X, Wang S, Zhang Z. Fluid–structure interaction investigation for coal-water slurry preheaters: Effects of different loads on mechanical performance. Numerical Heat Transfer, Part A: Applications. 2023;85:42-59 DOI: 10.1080/10407782.2023.2179558.

[7] Wang Q, Zhang Z, Wang F, Wu Z, Zheng Y, Lei D. Thermal stress and fatigue life analysis of absorber tubes in molten salt large-aperture parabolic trough collectors. Journal of Physics: Conference Series. 2025;3113:12045 DOI: 10.1088/1742-6596/3113/1/012045.

[8] Delibaş H, Yılmaz İH. A novel repair method for the lifespan and performance improvement of a shell-and-tube heat exchanger: A thermo-mechanical approach. Engineering Failure Analysis. 2025;170:109333.

[9] Štrucl J, Marn J, Zadravec M. Numerical modelling of conjugate heat transfer in force convective flow environment using a combined boiling model (CBM). Results in Engineering. 2025;26:104958 DOI: 10.1016/j.rineng.2025.104958.

[10] Maciunas V, Povilaitis M, Venckus J. CFD-Based Porous Media Approach for Optimizing Shell-and-Tube Heat Exchangers: Validation and Comparison of Baffle Configurations. ASME 2025 Heat Transfer Summer Conference. 2025 DOI: 10.1115/ht2025-156378.

[11] Nyong O, Ebieto C, Okara F, Obi E, Ene B. CFD Analysis of the Effect of Mass Flow Rate in a Shell and Tube Heat Exchanger Design. International Research Journal of Innovations in Engineering and Technology. 2024;8:215-20.

[12] Nyong OE, Igbong D, Ebieto C, Ene BE, Oluwadare B, Eso AA. Numerical simulation of two-phase gas-liquid flow through horizontal annulus pipe. Archives of Thermodynamics. 2023;44.

[13] Liao Y, Cai Q, He S, Wang M, Xiao H, Gong Z, et al. Study on three-dimensional numerical simulation of shell and tube heat exchanger of the surface ship under marine conditions. Nuclear Engineering and Technology. 2023;55:1233-43 DOI: 10.1016/j.net.2022.12.020.

[14] Nyong OE, Odu OE. Computer-based Program for Analyzing the Thermo-hydraulic Design of a Shell and Tube Heat Exchanger: Parametric Study. Computer. 2025;2.

[15] Hu Z, Wang H, Wang H, Shang Y, Pei Y, Li S, et al. High-temperature thermal fatigue of Ni3Al-based single crystal alloy affected by wall thickness and peak temperature. Journal of Materials Research and Technology. 2024;31:1582-95 DOI: 10.1016/j.jmrt.2024.06.149.

[16] Yue Z-Y, Yang X-X, Zhang Y-J, Pan D-X, Xu C. Numerical analysis of flow fields in a shell and tube heat exchanger. Thermal Science. 2023;27:1965-73 DOI: 10.2298/tsci2303965y.

[17] Bahiraei M, Naseri M, Monavari A. A CFD study on thermohydraulic characteristics of a nanofluid in a shell-and-tube heat exchanger fitted with new unilateral ladder type helical baffles. International Communications in Heat and Mass Transfer. 2021;124:105248.

[18] Biçer N, Engin T, Yaşar H, Büyükkaya E, Aydın A, Topuz A. Design optimization of a shell-and-tube heat exchanger with novel three-zonal baffle by using CFD and taguchi method. International Journal of Thermal Sciences. 2020;155:106417.

[19] Darbandi M, Abdollahpour M-S, Hasanpour-Matkolaei M. A new developed semi-full-scale approach to facilitate the CFD simulation of shell and tube heat exchangers. Chemical Engineering Science. 2021;245:116836.

[20] Wang S, He S, Wang M, Tian W, Su G, Qiu S. Two parallel methods for the three-dimensional CFD coupling simulation of shell and tube heat exchangers. Annals of Nuclear Energy. 2024;199:110374.

[21] Şahin M, Öztürk M. CFD analysis of the characteristic of a heat exchanger with counter flow shell tube under biogas-nanofluid conditions. Journal of Thermal Analysis and Calorimetry. 2025;150:9413-22.
[22] Muiz Abdul Raqib u, Yaser Alaiwi u, Ahmad Jundi u. Numerical Investigation of Thermal Performance Enhancement in a Newly Designed Shell and Tube Heat Exchanger using 〖"TiO" 〗_"2" Nanofluids. CFD Letters. 2024;17:60-82 DOI: 10.37934/cfdl.17.2.6082.
[23] Raut H. Investigation of Heat Transfer Rates on Shell and Tube Heat Exchanger by Numerical Modelling via CFD Analysis. undefined. 2023 DOI: 10.48550/ARXIV.2310.17257.
[24] Mogaji TS. Investigation of Tube Diameter and Baffle Thickness Effect on Shell and Tube Heat Exchanger Performance. null. 2020.
[25] Krisdiyanto K, Adi RK, Sudarisman S, Hamdan SB. An analysis of tube thickness effect on shell and tube heat exchanger. Eastern-European Journal of Enterprise Technologies. 2021;1:109.
[26] Ghazanfari V, Imani M, Shadman MM, Amini Y, Zahakifar F. Numerical study on the thermal performance of the shell and tube heat exchanger using twisted tubes and Al2O3 nanoparticles. Progress in Nuclear Energy. 2023;155:104526 DOI: 10.1016/j.pnucene.2022.104526.
[27] de Carvalho CAR, Marchi CH, Santiago CD. Richardson extrapolation with SubGrid to reduce the field discretization error in computational fluid dynamics. Journal of the Brazilian Society of Mechanical Sciences and Engineering. 2026;48:391 DOI: 10.1007/s40430-026-06370-1.
[28] Piasecka M, Piasecki A, Dadas N. Experimental Study and CFD Modeling of Fluid Flow and Heat Transfer Characteristics in a Mini-Channel Heat Sink Using Simcenter STAR-CCM+ Software. Energies. 2022 DOI: 10.3390/en15020536.
[29] Torri F, Berni F, Giacalone M, Mantovani S, Defanti S, Colombini G, et al. A methodology to reduce the computational effort in 3D-CFD simulations of plate-fin heat exchangers. Applied Thermal Engineering. 2024 DOI: 10.1016/j.applthermaleng.2024.122843.
[30] Zhu J, Frerich T, Herrmann A. CFD modeling and validation of heat transfer inside an autoclave based on a mesh independency study. Journal of Composite Materials. 2021;55:2469-87 DOI: 10.1177/0021998320979043.
[31] Wilcox DC. Turbulence modeling for CFD: DCW industries La Canada, CA; 1998.
[32] Ambekar AS, Sivakumar R, Anantharaman N, Vivekenandan M. CFD simulation study of shell and tube heat exchangers with different baffle segment configurations. Applied Thermal Engineering. 2016;108:999-1007.
[33] Arani AAA, Moradi R. Shell and tube heat exchanger optimization using new baffle and tube configuration. Applied Thermal Engineering. 2019;157:113736.
[34] Lam C, Bremhorst K. A modified form of the k-ε model for predicting wall turbulence. 1981.
[35] Launder BE, Spalding DB. The numerical computation of turbulent flows. Numerical prediction of flow, heat transfer, turbulence and combustion: Elsevier; 1983. p. 96-116.
[36] Van Driest ER. On turbulent flow near a wall. Journal of the aeronautical sciences. 1956;23:1007-11.